

Using density matrix quantum Monte Carlo for calculating exact-on-average energies for ab-initio Hamiltonians in a finite basis set

Hayley R. Petras,^{†,‡} Sai Kumar Ramadugu,^{†,‡} Fionn D. Malone,[¶] and James J. Shepherd^{*,†,‡}

[†]*Department of Chemistry, University of Iowa*

[‡]*University of Iowa Informatics Initiative, University of Iowa*

[¶]*Quantum Simulations Group, Lawrence Livermore National Laboratory, 7000 East Avenue, Livermore, CA, 94551 USA.*

E-mail: james-shepherd@uiowa.edu

Abstract

We here apply the recently developed initiator density matrix quantum Monte Carlo (i-DMQMC) to a wide range of chemical environments using atoms and molecules in vacuum. i-DMQMC samples the exact density matrix of a Hamiltonian at finite temperature and combines the accuracy of full configuration interaction quantum Monte Carlo (FCIQMC) full configuration interaction (FCI) or exact energies in a finite basis set with finite temperature. By way of exploring the applicability of i-DMQMC for molecular systems, we choose to study a recently developed test set by Rubenstein and coworkers: Be, H₂O, and H₁₀ at near-equilibrium and stretched geometries. We find that, for Be and H₂O, i-DMQMC delivers energies which are sub-millihartree accuracy when compared with finite temperature FCI. For H₂O and both geometries of

H_{10} we examine the difference between FT-AFQMC and i-DMQMC which in turn is an estimate of the difference in canonical versus grand canonical energies. We close with a discussion of simulation parameters (initiator error and different basis sets) and by showing energy difference calculations in the form of specific heat capacity and ionization potential calculations.

December 3, 2019

1 Introduction

The last decade has seen a remarkable growth in the study of warm dense matter.^{1,2} Encompassing conditions intermediate between plasma and condensed matter physics, warm dense matter is relevant to the study of planetary interiors^{3,4}, hot-electron chemistry⁵ and laser excited solids⁶. Experimentally, warm dense matter can now be routinely investigated in large scale laser facilities⁷. However, the theoretical description of warm dense matter is challenging due to equal importance of electron-electron, quantum degeneracy and thermal electronic effects. Finite temperature density functional theory (FT-DFT)⁸, coupled with molecular dynamics, is currently the method of choice, due to its relatively low computational cost and often satisfactory agreement with experiment⁹. However, unlike its ground state counterpart, there is not the same level of understanding of its limitations and dependence on the form of exchange correlation free energy functional used^{10–13}. Thus, there is a need to develop more accurate approaches which can benchmark, and potentially supplement FT-DFT.

Much like the more familiar zero temperature wavefunction-based quantum chemistry methods there is in principle a hierarchy of finite temperature methods starting with thermal Hartree–Fock theory¹⁴ and ending in finite temperature full configuration interaction theory¹⁵. The performance of this hierarchy of approaches in a quantum chemical context have only recently begun to be explored. For example, finite temperature perturbation the-

ories^{16,17}, Green's function methods¹⁸ as well as coupled cluster theory^{19,20} have all been developed in recent years with promising results. Other approaches include thermofield theory²¹ with extensions to time-dependent coupled cluster²² and cumulant-based approaches²³.

Quantum Monte Carlo (QMC) methods offer an alternative stochastic approach to simulating systems at finite temperature. QMC methods are attractive as they offer a favourable scaling with system size $\mathcal{O}(N^3 - N^4)$ and can scale on modern supercomputing architectures. Unfortunately, they also suffer from the fermion sign problem at low temperatures and large system sizes that can only be overcome at polynomial cost by imposing a constraint. The bias resulting from this constraint, while typically small, can only be systematically removed at an exponential cost in general.

Of the finite temperature QMC methods available, real space path integral Monte Carlo (PIMC) is perhaps the most widely used²⁴. It has the significant advantage of working in the complete basis set limit which is otherwise challenging to reach at finite temperature due to the thermal occupation of virtual states. As a result, PIMC is already a standard method in the simulation of warm dense matter^{25,26}. To overcome the sign problem at low temperature, one can use the restricted path integral formalism (RPIMC)²⁷, similar in spirit to the fixed-node approximation in diffusion Monte Carlo (DMC)²⁸, which enforces a constraint using a trial density matrix. The quality of this constraint is largely unknown, however results for the uniform electron gas suggest it is unreliable at high densities and at lower temperatures^{29–31}. We note there have been promising developments in extending the scope of PIMC to lower temperatures and higher densities through algorithmic developments^{32–34}.

Auxiliary-Field QMC (AFQMC) is another promising QMC method capable of simulating matter at finite temperature^{35–38}. In contrast to PIMC, AFQMC works in a second quantized framework, utilizing the Hubbard-Stratonovich transformation to write the partition function as an integral over auxiliary fields of fermion determinants. Motivated by the remarkable accuracy of AFQMC for the ground state properties of model Hamiltonians and ab-initio systems^{39–41}, Liu *et al.* recently extended the finite temperature phaseless AFQMC

algorithm⁴² to simulate ab-initio systems and developed a set of molecular benchmarks for small atoms and molecules for which no constraint was required.⁴³ Each of these systems had its temperature-dependent internal energy calculated in the grand canonical ensemble, in a vacuum, and also in a finite basis set: Be (MIDI) atom, H₂O (STO-3G) molecule, C₂ (STO-6G) molecule, H₁₀ (STO-6G), and stretched H₁₀ (STO-6G). This interesting test set deserves attention because it represents a range of different chemical environments, incorporating both weak and strong correlation.

In this paper we investigate the ability of an alternative QMC method, the density matrix quantum Monte Carlo method (DMQMC)⁴⁴ in its initiator variant³¹ (i-DMQMC) to simulate real ab-initio systems. DMQMC is the finite temperature analogue of the full configuration interaction QMC method (FCIQMC)⁴⁵ and is capable of simulating systems outside the reach of conventional FCI without imposing a constraint. To date, DMQMC has been applied to simulate the 2D-Heisenberg model⁴⁴ and the warm dense uniform electron gas^{31,46}, however its performance for real systems is largely unknown. DMQMC is a promising tool in the benchmarking of finite temperature methods as it provides access to a statistical representation of the N -electron thermal density matrix. Thus, arbitrary expectation values can be evaluated as well as free energy differences³¹ and Renyi entropies⁴⁴ which are often a challenge for QMC methods. Moreover, it can build on the many advancements made in the FCIQMC community such as the initiator approximation⁴⁷, semi-stochastic approaches^{48,49}, better excitation generators^{50,51}, and perturbative corrections^{52,53}. Additional exciting advancements based on coupled cluster equations include cluster-analysis-driven FCIQMC (CAD-FCIQMC) for accelerating convergence of FCIQMC,⁵⁴ as well as the EOMCC(P) approach, that uses the early stages of FCIQMC to converge excited state energies at the EOMCCSD(T) level of theory.⁵⁵. Stochastic approaches that build off of the deterministic CC(P;Q) methodology have also been developed.⁵⁶⁻⁵⁸

Given that the scope of benchmark systems accessible to FCIQMC includes the UEG, as well as atoms, ions, molecules, dimers, and most recently, solids⁵⁹, it is important to

investigate to what extent DMQMC follow this success. To begin answering this question, we present a set of calculations on previously established benchmark systems.

Our paper is organized as follows: In Section 2, we present a brief overview of the DMQMC method, following the derivation from Blunt and coworkers⁴⁴ and including the initiator approximation to DMQMC. Section 3 presents the comparison of full configuration interaction to i-DMQMC, a comparison to FT-AFQMC, a demonstration of the initiator approximation in DMQMC, i-DMQMC results for H₂O in three finite basis-sets and finally, additional applications of finite-temperature results. In Section 4, we conclude with final thoughts and future work.

2 Methods

Following the derivation from Blunt and coworkers,⁴⁴ it can be shown that the N -particle density matrix in the canonical ensemble can be sampled by solving the symmetrized Bloch equation using a stochastic approach. Starting with the thermal density matrix

$$\hat{\rho}(\beta) = e^{-\beta \hat{H}}, \quad (1)$$

where \hat{H} is the Hamiltonian operator and $\beta = \frac{1}{k_B T}$ is the inverse temperature, differentiation with respect to β shows that the density matrix obeys the symmetrized Bloch equation

$$\frac{d\hat{\rho}(\beta)}{d\beta} = -\frac{1}{2}(\hat{H}\hat{\rho} + \hat{\rho}\hat{H}) = -\frac{1}{2}\{\hat{H}, \hat{\rho}\}. \quad (2)$$

The density matrix at any temperature can then be found using a finite difference approach:

$$\hat{\rho}(\beta + \Delta\beta) = \hat{\rho}(\beta) - \frac{\Delta\beta}{2}(\hat{H}\hat{\rho}(\beta) + \hat{\rho}(\beta)\hat{H}) + O(\Delta\beta^2) \quad (3)$$

where a finite time step $\Delta\beta$ has been introduced. Eq. (3) coupled with the the initial condition $\hat{\rho}(\beta = 0) = \hat{I}$ is sufficient to determine to density matrix at any temperature.

To proceed we represent the density matrix in a basis of outer products of Slater determinants and rewrite Eq. (3) as

$$\rho_{ij}(\beta + \Delta\beta) = \rho_{ij}(\beta) + \Delta\rho_{ij}(\beta) \quad (4)$$

$$\begin{aligned} \Delta\rho_{ij}(\beta) &= -\frac{\Delta\beta}{2} \sum_k [(H_{ik} - S\delta_{ik})\rho_{kj} - \rho_{ik}(H_{kj} - S\delta_{kj})] \\ &= \frac{\Delta\beta}{2} \sum_k (T_{ik}\rho_{kj} + \rho_{ik}T_{kj}). \end{aligned}, \quad (5)$$

where $\rho_{ij} = \langle D_i | \hat{\rho} | D_j \rangle$ and $|D_i\rangle$ is a Slater determinant, S is a variable shift to be defined, and $T_{ij} = -(H_{ij} - S\delta_{ij})$. The idea of DMQMC is to now introduce a population of N_w signed walkers which sample elements of the density matrix and evolve according to (5). At $\beta = 0$ walkers are uniformly distributed among the diagonal density matrix elements. At each time step walkers then undergo a series of spawning cloning/death and annihilation steps analogous to those in FCIQMC. Spawning is the probability a particle will spawn from a density matrix element ρ_{ik} to ρ_{ij} and is given as $p_s(ik \rightarrow ij) = \frac{\Delta\beta|T_{kj}|}{2}$, with $\text{sign}(\rho_{ij}) = \text{sign}(\rho_{ik}) \times \text{sign}(T_{kj})$, with a similar expression for $p_s(kj \rightarrow ij)$. The cloning/death process, where the number of walkers on a given density matrix element is either increased or decreased, is given by probability of $p_d(ij) = \frac{\Delta\beta}{2}|T_{ii} + T_{jj}|$. The particles clone if $\text{sign}(T_{ii} + T_{jj}) \times \text{sign}(\rho_{ij}) > 0$ and die otherwise. To help control the sign problem, particles of opposite signs on the same density matrix element are annihilated; this annihilation does not affect the distribution of particles. Similar to other QMC methods we must use population control to avoid either a population explosion or collapse. We use a variable shift, S , which is adjusted according to

$$S(\beta + A\Delta\beta) = S(\beta) - \frac{\zeta}{A\Delta\beta} \ln \left(\frac{N_w(\beta) + A\Delta\beta}{N_w(\beta)} \right) \quad (6)$$

where A is the number of beta steps between shift updates, ζ is a shift damping parameter,

$N_w(\beta)$ is the total number of walkers at β . The shift damping parameter is chosen by the user when necessary to prevent large fluctuation in the shift. This process is repeated until a desired inverse temperature is reached. One complete evolution of walkers is called a β -loop and we average results over many such (independent) β -loops to obtain statistical estimates for physical observables.

At a specific temperature, the quantum mechanical expectation value for any quantum mechanical operator, \hat{O} , can be found through the stochastic sampling of

$$\langle \hat{O} \rangle = \frac{\text{Tr}(\hat{\rho}\hat{O})}{\text{Tr}(\hat{\rho})} = \frac{\frac{1}{N_\beta} \sum_{\alpha}^{N_\beta} \sum_{ij} w_{ij}^{(\alpha)} O_{ji}}{\frac{1}{N_\beta} \sum_{\alpha}^{N_\beta} \sum_i w_{ii}^{(\alpha)}}, \quad (7)$$

where $w_{ij}^{(\alpha)}$ is the walker population on ρ_{ij} for simulation α of N_β β -loops and the β dependence has been omitted from the expression for clarity. The numerator and denominator are sampled separately over the course of the evolution, and the average for each value is calculated at discrete temperature values. Calculations are averaged over a number of β -loops until the desired statistical accuracy is achieved.

The goal of the initiator approximation for DMQMC (i-DMQMC)³¹ is similar to that of i-FCIQMC⁶⁰: Restrict the spawning of walkers from negligibly small elements to other negligibly small elements. A threshold is set to determine "initiator determinants", where the walker population on those elements are higher than that of the threshold. The approximation then restricts the algorithm such that only the "initiator determinants" can spawn children onto unoccupied matrix elements. Children can also be spawned from multiple sign-coherent events. In the infinite population limit, the initiator approximation is recovered as the orginal DMQMC algorithm.

The DMQMC calculations that follow used a timestep of 0.001 (Ha⁻¹). The target population was chosen to be 5×10^6 ; we show in section IIIA that the finite-temperature results are converged at a target population of 10^6 , similar to FCIQMC. We found that 25 β -loops gave us the desired statistical accuracy without being overly computationally

demanding. Each calculation completed in less than a week. All of the calculations that follow were performed with the initiator approximation to DMQMC (*i*-DMQMC)³¹, unless noted otherwise. All calculations were performed using the HANDE code⁶¹.

3 Results

To assess the capabilities of *i*-DMQMC on small molecules, we have performed a series of simulations on a small set of systems. We first present a comparison to finite temperature and ground state full configuration interaction (FCI) for Be and H₂O to assess the accuracy of the method, and show that *i*-DMQMC can treat small molecules and atoms without modifications such as importance sampling⁴⁴ or the interaction picture⁴⁶. We then provide a comparison of H₂O in the canonical (*i*-DMQMC) and grand canonical ensembles (FT-AFQMC). Next, we investigate the rate of convergence of *i*-DMQMC with respect to target population and show *i*-DMQMC results for H₂O in a variety of basis-sets to determine the ease of applicability of *i*-DMQMC to molecular systems. Finally, due to the small errors in the *i*-DMQMC results, we investigate additional applications of *i*-DMQMC , where we show that we can take energy differences and calculate properties such as specific heat and ionization energy as functions of temperature.

3.1 Agreement between **i**-DMQMC and FCI

In this section we first compare our *i*-DMQMC results on small molecules to FT-FCI. For such small systems, we can determine all eigenstates of the Hamiltonian and compute the temperature-dependent internal energy (*U*) using: $\langle \hat{H} \rangle = \frac{\sum_i E_i e^{-\beta E_i}}{\sum_i e^{-\beta E_i}}$, where *E_i* is an eigenvalue of the FCI Hamiltonian computed in a given basis set.

In Fig. 1, *i*-DMQMC is compared with FT-FCI for (a) the beryllium atom in the MIDI basis set and (b) H₂O in the STO-6G basis set. The energies were calculated for a range of inverse temperatures ($0.01 \leq \beta \leq 35.00$) and averaged over 25 β -loops. Both i-DMQMC

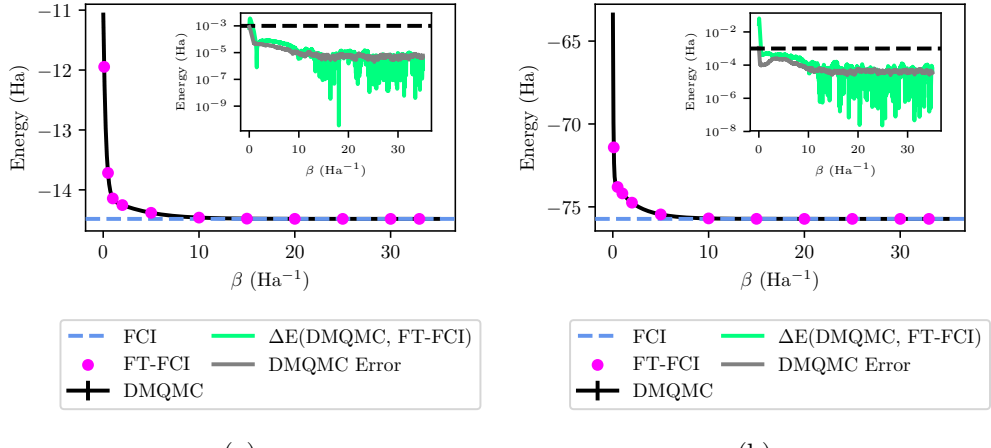


Figure 1: The energy of the (a) Be atom (MIDI) and (b) H_2O (STO-6G) at various inverse temperatures using i -DMQMC (black), FT-FCI (magenta) and ground state FCI (blue). The integral files were generated in pySCF⁶²; H_2O was generated with an O–H bond length of 0.96 Å and a bond angle of 109.5 degrees. The error bars are plotted in the main graph, but may be too low to see their actual scale. The inset presents the statistical errors (grey) more clearly, as well as the absolute difference between FT-FCI and i -DMQMC (green), plotted on a logarithmic y-axis. As a reference, a black dashed line is provided in the inset at 10^{-3} . FCI results were obtained using the FCI routine in HANDE-QMC; FT-FCI is described in the text. The i -DMQMC simulation was run with a timestep of 0.001 Ha^{-1} , the target population was set to 5×10^6 , and run to $\beta = 35$.

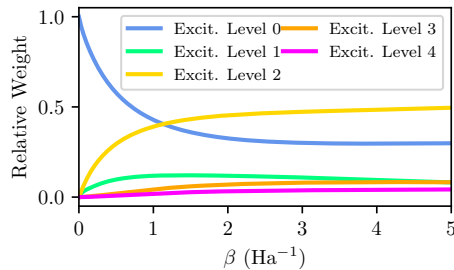


Figure 2: The relative weights of matrix elements in a single β -loop simulation of H_2O (STO-6G). The i -DMQMC simulation was run with a timestep of 0.001 Ha^{-1} , the target population was set to 5×10^6 , and run to $\beta = 5$. The higher the relative weight in, the more off-diagonal the element is.

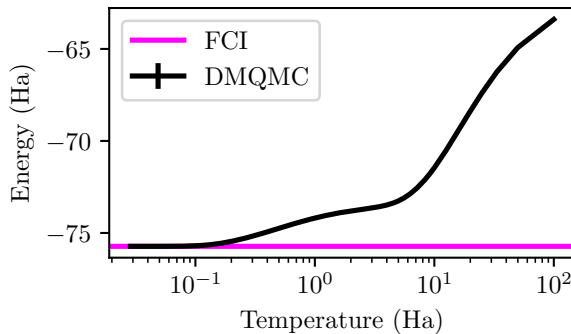


Figure 3: The i-DMQMC results for H_2O (STO-3G, black) as a function of *temperature*, plotted on a logarithmic x-axis, with the ground state FCI value (magenta) shown for comparison. The statistical error is plotted for the i-DMQMC result, but is invisible on this scale.

and FT-FCI can be computed straightforwardly for these systems so the sampling in β can be made arbitrarily fine. As can be seen in both figures, the FT-FCI points agree with the *i*-DMQMC calculations to within the *i*-DMQMC statistical error bar ($\pm\sigma_{\bar{U}}$), indicating that the systematic error has been eliminated to at least below the statistical error. *i*-DMQMC and ground state FCI values agree within 2σ at $\beta > 5$. At $\beta < 5$, the deviations are larger but the energy gap is still small relative to the total energy. The statistical error bar in the *i*-DMQMC calculation is invisible on the graphs as shown but has been added as an inset. The errors in both the Be and H_2O systems are sub-milliHartree, and a dashed line has been provided on the insets at 10^{-3} as a reference. The *i*-DMQMC and FCI errors are the same order of magnitude, and although the difference is greater than the error at some points, we attribute this to an error in the error calculation.

We used 25 β loops for these simulations in order to achieve error bars of the desired accuracy ; this is a significantly lower number of loops than previous studies but we wanted to consider what was a typical cost-effective simulation.⁴⁴ The time taken to run the *i*-DMQMC simulation on H_2O to $\beta = 35$ over 25 β -loops is 110 core-hours.

The relative weights for each state in a single β -loop simulation on H_2O are shown in Fig. 2, for $0.00 < \beta \leq 5.00$ where the higher the relative weight, the more off diagonal the element is. It can be seen from this plot that the relative weight of the diagonal (excitation

level 0) dominates the simulation at $\beta < 1$. The off-diagonal elements, besides excitation level 2, have low relative weights, showing the sparsity of the density matrix. This is significant because analyzing the distribution of weights in the density matrix can provide information for other methods that utilize trial density matrices, such as AFQMC.

In Fig. 3, we show the i -DMQMC energy for H_2O as a function of *temperature*, compared to the ground state FCI energy. We expect the i -DMQMC energy to converge to the FCI ground state in the zero-temperature limit, and this is confirmed in the plot. This is a critical test for finite-temperature methods to assess the accuracy of the method because if the simulation does not converge to the ground state FCI energy in the zero temperature limit, then this is indicative of a sampling error. Our prior work investigated this in the context of the uniform electron gas.³¹ As the temperature approaches zero, the energy we obtain using i -DMQMC approaches the FCI energy which is seen both in this figure and in Fig. 1(b), where the i -DMQMC result overlaps with the ground state FCI. At temperatures lower than 0.1 Ha, the statistical error in i -DMQMC makes it impossible to distinguish the energy difference from zero. These results are noteworthy in light of the fact that we have not yet applied algorithmic improvements beyond the initiator approximation; in future studies it would be interesting to see the effect of importance sampling⁴⁴ or the interaction picture.⁴⁶ By showing agreement between i -DMQMC and ground state FCI at the zero temperature limit, as well as agreement between FT-FCI and the i -DMQMC results, we have shown evidence that strongly suggests i -DMQMC is a highly accurate method for treating small molecular and atomic systems.

3.2 Comparison to AFQMC

Due to the success of the recently developed finite-temperature auxiliary field quantum Monte Carlo (FT-AFQMC) method for small molecules, atoms, solids and models, we choose to directly compare our results for an equilibrium and stretched H_{10} molecule (STO-6G) and H_2O (STO-3G) to Rubenstein and coworkers.⁴³ One significant difference between the

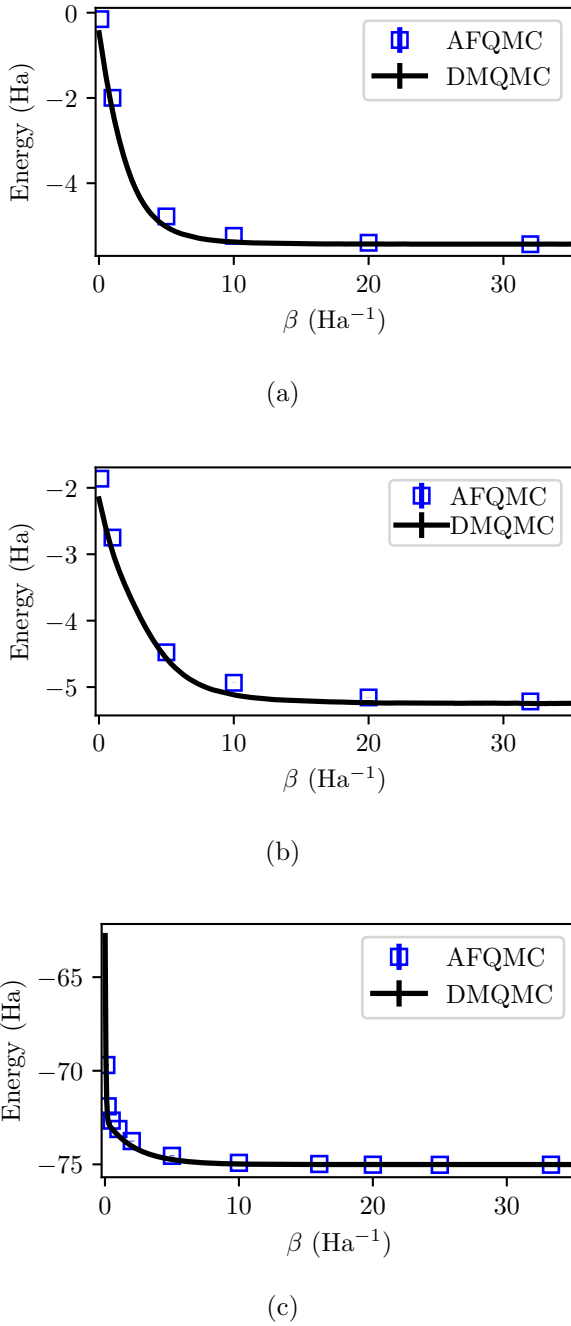


Figure 4: The i -DMQMC results of (a) equilibrium H_{10} , (b) stretched H_{10} and (c) H_2O (STO-3G) compared to FT-AFQMC at discrete values of β . The equilibrium H_{10} has a bond length of 1.786 Å and the stretched H_{10} molecule has a bond length of 2.4 Å and was generated using the STO-6G basis set. The integral files for the H_{10} systems were generated in MOLPRO⁶³.

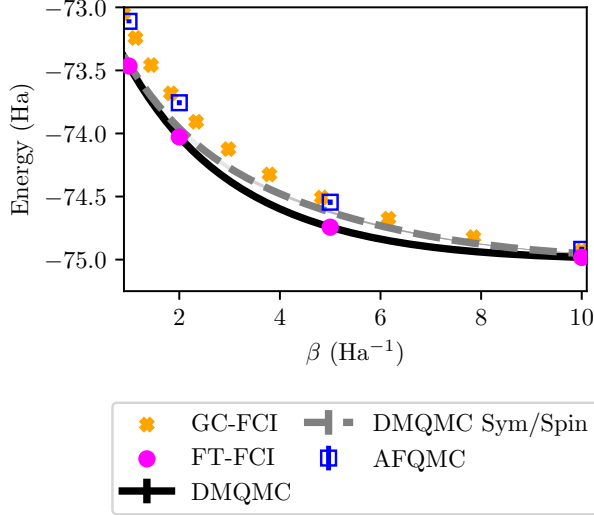


Figure 5: The energy results of three different methods: i —DMQMC (black), i —DMQMC, sampled over all symmetries and spin polarizations (grey, dotted); GC-FCI (orange crosses); FT-FCI (magenta circles) and FT-AFQMC (blue squares). The same H_2O geometry was used for these calculations as above, but the integral was produced in the STO-3G basis set for comparison with Rubenstein and coworkers. The i —DMQMC calculation details can be found in the main text.

i —DMQMC method utilized here and the FT-AFQMC used by Rubenstein and coworkers is that they are performed in different ensembles. FT-AFQMC works in the grand canonical ensemble, while i -DMQMC works in the canonical ensemble. It is possible for both of these methods to work in each of the two ensembles, but this is not addressed here. We note that differences between the two ensembles are expected to be most pronounced in the small systems studied here.

We present FT-AFQMC results, as reported by Rubenstein and coworkers,⁴³ in comparison with i —DMQMC results in Fig. 4 for H_{10} , stretched H_{10} and H_2O (STO-3G) in the range of $0.01 \leq \beta \leq 35.00$. The difference between the FT-AFQMC and the i —DMQMC results cannot be seen clearly in this figure, because the energy differences are small on this scale. The greatest differences are at low values of β for each of the three systems. For H_2O the highest difference occurs at 0.1 Ha^{-1} , where the absolute difference between the two methods is approximately 1.01 Ha. The difference between the two methods decreases as β increases, which suggests they are both converging to the zero-temperature limit.

In Fig. 5 we have plotted both grand canonical FCI (GC-FCI) and FT-FCI results with

the FT-AFQMC and i -DMQMC results for an intermediate β range. The FT-AFQMC agrees with the GC-FCI results, as is to be expected, while the FT-FCI results agree with the i -DMQMC simulations.

To investigate whether the differences between the i -DMQMC and FT-AFQMC results is indeed an artifact of ensemble differences, the internal energy of H_2O was also calculated in Fig. 5 wherein all spin sectors are sampled over (DMQMC Sym/Spin), as opposed to the usual case when only elements with $M_s = 0$ are sampled. As can be seen from the figure, this approximation is well controlled with the effect of spin sampling being most noticeable in intermediate β ranges.

3.3 Initiator error and basis sets

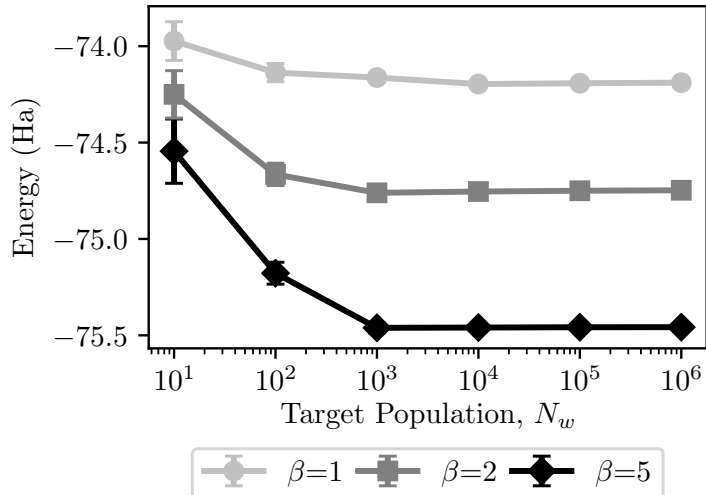


Figure 6: The i -DMQMC energies of H_2O (STO-6G) at $\beta = 1$ (circles), $\beta = 2$ (squares) and $\beta = 5$ (diamonds), as a function of target population. i -DMQMC was performed with 6 different target populations of 10 to 10^6 in logarithmic steps. The error bars are plotted for each marker, but may be invisible on this scale for the larger target populations.

The initiator approximation is used in i-DMQMC to exploit the sparsity of the density matrix by controlling the ability of walkers to spawn from very small matrix elements to other small elements,³¹ as adapted from the FCIQMC initiator method.⁶⁰ The initiator approximation was designed to restrict spawning from negligibly small matrix elements to other

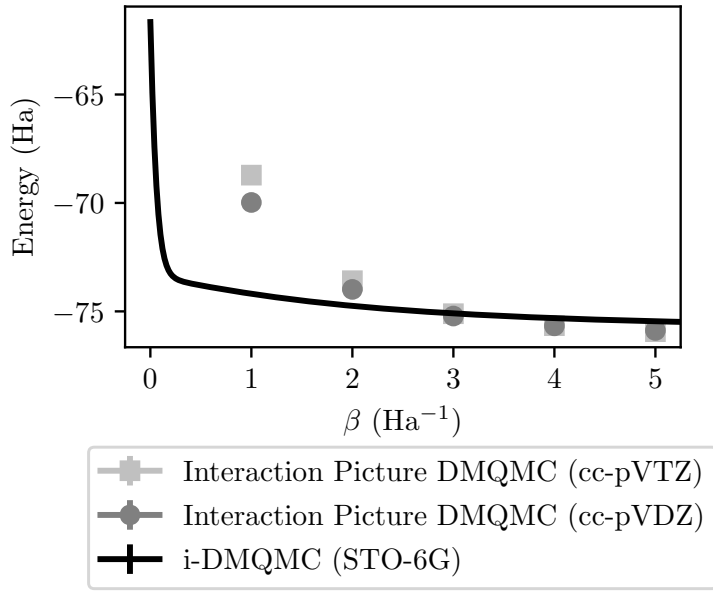


Figure 7: Energy results for $0.01 \leq \beta \leq 5.00$ for H_2O in three basis sets: STO-6G (black), cc-pVDZ (grey circles) and cc-pVTZ (light grey squares). The number of orbitals in each basis set for H_2O is 7, 24 and 58, respectively. . The results for cc-pVDZ and cc-pVTZ were obtained using the interaction picture variant of DMQMC⁴⁶. The simulations were run over 25 β -loops. The interaction picture calculations were performed with a timestep of 0.0001 Ha^{-1} and a target population of 10^5 .

small matrix elements. This is accomplished by setting a n_{add} , a threshold that determines a set of "initiator determinants", where particles can only be spawned to unoccupied matrix elements if the particles originate from the set of elements with a population greater than n_{add} . Here, $n_{add} = 3.0$.

In Figure 6 we compare the rate of convergence for three values of β with respect to target population for i -DMQMC. The energy decreases with increasing target population until the energy is converged. As shown in the plot, the results for $\beta=2$ and $\beta=5$ converge at a target population of 10^3 . The absolute differences between $N_w=10^3$ and $N_w=10^4$ for $\beta=2$ and $\beta=5$ are 0.007 Ha and 0.001 Ha respectively. $\beta=1$ converges at a slightly higher population of 10^4 , and the absolute difference between $N_w=10^4$ and $N_w=10^5$ is 0.004 Ha. For this target population range, the error is visible for $N_w=10$ and $N_w=10^2$, but decreases as N_w increases, such that the error bar becomes invisible on this scale. We can see from the relatively fast convergence rate and decreasing error, that i -DMQMC is well-controlled with respect to target population. This data suggests that the i -DMQMC energy converges similarly to i-FCIQMC with respect to target population, and is a vital part of showing the validity of this method in the long-term.

Fig. 7 compares the i -DMQMC results of H_2O in the STO-6G basis set compared to the interaction picture i -DMQMC results in the cc-pVDZ and cc-pVTZ basis sets. The interaction picture is a modification to the original DMQMC algorithm that was developed to stabilize sampling in larger basis sets at the cost of only sampling one β at a time.⁴⁶ We see that the internal energy converges with basis set differently depending on the β value. At high temperatures the internal energy increases which is caused by the increase in kinetic energy as higher single-particle states become occupied. As the temperature is decreased (large β) we see that increasing the basis set size serves to lower the internal energy, which is to be expected as we approach the $T = 0$ limit. Comparing the three basis-sets, we see that i -DMQMC controls the error for all three relatively well. This is similar to FCIQMC and shows promise for the applicability of i -DMQMC to molecular systems. The use of

interaction picture DMQMC has not yet been studied extensively; that work is out of the scope of this paper, but is a future line of inquiry.

3.4 Applications with energy differences

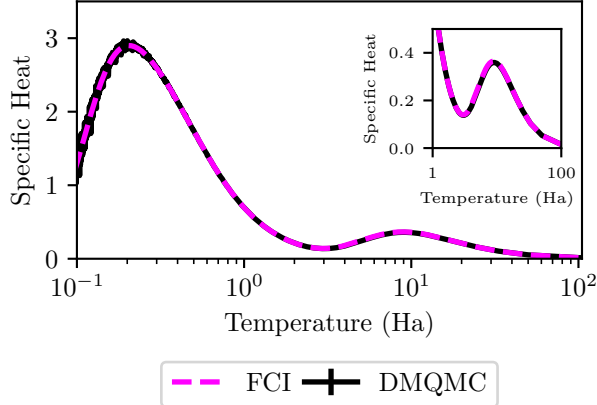


Figure 8: The specific heat of H_2O , calculated numerically as described in the text, from the internal energy output of the i -DMQMC calculation (black) and from FT-FCI (magenta). Note the specific heat presented is dimensionless because DMQMC works in atomic units. The specific heat is presented as a function of temperature, with temperature on a logarithmic scale in order to see the low temperature limit with more detail. The propagated error is plotted for the i -DMQMC result, but is invisible on this scale.

The internal energy is not the only physical observable that can be studied from the i -DMQMC method. We demonstrate here that due to the small errors, this method is a strong candidate for taking energy differences, such as those that are used for calculating numerical derivatives and those used for calculating the ionization energy of atoms and molecules. We show the specific heat as a function of temperature can be calculated from i -DMQMC with accuracy at the FT-FCI level.

The specific heat, C_V , was computed from the usual expression

$$C_V = \left(\frac{\partial U}{\partial T} \right)_V = -\frac{1}{k_B T^2} \left(\frac{\partial U}{\partial \beta} \right)_V, \quad (8)$$

where we used finite-differences to numerically compute the derivative of the internal energy. The results for the specific heat of H_2O in the STO-6G basis-set, are shown in Fig. 8 for both

i-DMQMC and FT-FCI. By visual inspection, the curves overlap exactly, which is indicative of the two methods being in agreement. The specific heat of H₂O in two larger basis sets, cc-pVDZ and cc-pVTZ, were also investigated, and the results of these plots showed a similar shape to the STO-6G data, but the noise is overwhelming at higher temperature values than that of the STO-6G results. At lower temperature this procedure became overwhelmed by noise, which is to be expected due to issues differentiating stochastic functions⁶⁴. A more direct approach, would be to compute $\frac{1}{k_B T^2}(\langle \hat{H}^2 \rangle - \langle \hat{H} \rangle^2)$ directly in the simulation, however this would be computationally challenging and we did not attempt it here.

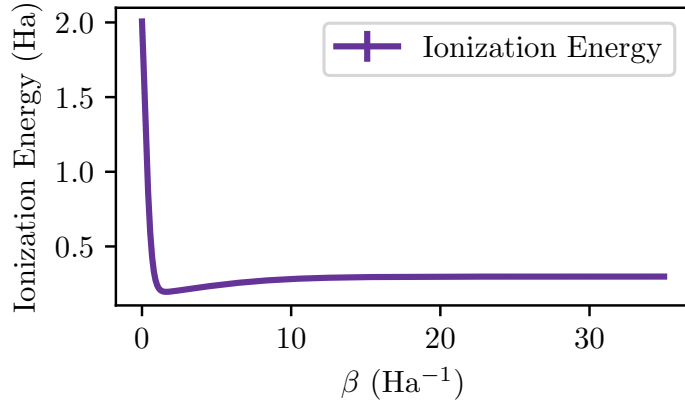


Figure 9: The ionization potential for Be as a function of inverse temperature ($0.01 \leq \beta \leq 35.00$). Two calculations were performed, one on Be and one on Be⁺, both in the MIDI basis set. The propagated error is plotted, but is invisible on this scale.

In Fig. 9 we plot the energy difference, $\Delta U = U_{\text{Be}^+} - U_{\text{Be}}$, representing the first ionization potential of Be. As can be seen from the plot, the calculated ionization energy is less than 0.5 Ha for most values of β , which indicates a method with milliHartree accuracy is needed in order to accurately capture energy differences such as ionization potential. We hope to extend this procedure in future work by investigating high oxidation states of transition metals.

We have shown *i*-DMQMC is well-equipped for calculating properties than involve energy differences. The stochastic nature of *i*-DMQMC gives good control of the noise in the calculation, allowing for calculated differences between energy to be physically significant.

4 Conclusions

The main achievement of the DMQMC method to date has been to treat model systems such as the 2d-Heisenberg model⁴⁴ and the uniform electron gas.³¹ In the latter, DMQMC was recently used to benchmark the warm dense electron gas with implications to finite density temperature functionals.³¹ In these systems it has shown that Hilbert spaces of significant system sizes can be treated with exact-on-average accuracy.

In this paper, we took a first look at DMQMC as it applies to ab initio systems. We aimed to reproduce the same series of calculations presented by Rubenstein et al. who used FT-AFQMC on Be, H₂O, and H₁₀ at near-equilibrium and stretched geometries. We successfully showed that i-DMQMC can reproduce FCI results within 1 millihartree (stochastic and systematic error) for Be and H₂O for a wide range of inverse temperatures. The initiator error was shown to be well-controlled by raising the walker population size. In comparing i-DMQMC with FT-AFQMC, we were able to benchmark the difference between the grand canonical ensemble and canonical ensemble energies for finite systems, specifically, for H₂O and H₁₀ at near-equilibrium and stretched geometries. Finally, we demonstrated that it was possible to take numerical differences between i-DMQMC results since the stochastic noise is sufficiently well-controlled.

The DMQMC method is a close relation to FCIQMC⁴⁵ and, as such, it remains an open question as to whether DMQMC can have the same success in treating systems with larger system sizes. We note that we have left open the question of how the method scales, although it is anticipated that it will scale in a similar fashion to FCIQMC.⁶⁵ In the early days of FCIQMC, it went through significant development that saw it reduce the scaling of the method considerably and it is hoped that with sufficient attention DMQMC may be able to follow suit. Another way that DMQMC could find a niche is if it can treat (and benchmark) finite temperature energies for solids, which appears to be one of the large open questions in finite temperature electronic structure theory. We are indeed interested in this question and it will be investigated in future work which is forthcoming.

5 Acknowledgements

JJS, SKR, and HRP acknowledge the University of Iowa for funding. The work of FDM was performed under the auspices of the U.S. Department of Energy (DOE) by LLNL under Contract No. DE-AC52-07NA27344. Computer time was provided by the Livermore Computing Facilities and the University of Iowa Informatics Initiative. The code used throughout this work was HANDE (www.hande.org.uk). We gratefully acknowledge Maciej Jarocki for preliminary work in this area and Matthew Foulkes for discussions at Imperial College London. We would also like to thank Brenda Rubenstein and Yuan Liu for discussions and access to the 1.786 ÅH₁₀ and 2.4 ÅH₁₀ integral files used in their paper.⁴³

References

- (1) Graziani, F.; Desjarlais, M. P.; Redmer, R.; Trickey, S. B. *Frontiers and Challenges in Warm Dense Matter*; Springer Science & Business, 2014; Google-Books-ID: Hdm4BAAAQBAJ.
- (2) Dornheim, T.; Groth, S.; Bonitz, M. The uniform electron gas at warm dense matter conditions. *Physics Reports* **2018**, *744*, 1 – 86.
- (3) Benuzzi-Mounaix, A.; Mazevert, S.; Ravasio, A.; Vinci, T.; Denoeud, A.; Koenig, M.; Amadou, N.; Brambrink, E.; Festa, F.; Levy, A.; Harmand, M.; Brygoo, S.; Huser, G.; Recoules, V.; Bouchet, J.; Morard, G.; Guyot, F.; Resseguiier, T. d.; Myanishi, K.; Ozaki, N.; Dorchies, F.; Gaudin, J.; Leguay, P. M.; Peyrusse, O.; Henry, O.; Raffestin, D.; Pape, S. L.; Smith, R.; Musella, R. Progress in warm dense matter study with applications to planetology. *Physica Scripta* **2014**, *T161*, 014060, bibtex: benuzzi-mounaix_progress_2014.
- (4) Koenig, M.; Benuzzi-Mounaix, A.; Ravasio, A.; Vinci, T.; Ozaki, N.; Lepape, S.; Batani, D.; Huser, G.; Hall, T.; Hicks, D.; MacKinnon, A.; Patel, P.; Park, H. S.;

Boehly, T.; Borghesi, M.; Kar, S.; Romagnani, L. Progress in the study of warm dense matter. *Plasma Physics and Controlled Fusion* **2005**, *47*, B441.

(5) Mukherjee, S.; Libisch, F.; Large, N.; Neumann, O.; Brown, L. V.; Cheng, J.; Lasiter, J. B.; Carter, E. A.; Nordlander, P.; Halas, N. J. Hot Electrons Do the Impossible: Plasmon-Induced Dissociation of H₂ on Au. *Nano Letters* **2013**, *13*, 240–247.

(6) Ernstorfer, R.; Harb, M.; Hebeisen, C. T.; Sciaiani, G.; Dartigalongue, T.; Miller, R. J. D. The Formation of Warm Dense Matter: Experimental Evidence for Electronic Bond Hardening in Gold. *Science* **2009**, *323*, 1033–1037, bibtex: ernstorfer_formation_2009.

(7) Fletcher, L. B.; Lee, H. J.; Döppner, T.; Galtier, E.; Nagler, B.; Heimann, P.; Fortmann, C.; LePape, S.; Ma, T.; Millot, M.; Pak, A.; Turnbull, D.; Chapman, D. A.; Gericke, D. O.; Vorberger, J.; White, T.; Gregori, G.; Wei, M.; Barbrel, B.; Falcone, R. W.; Kao, C. C.; Nuhn, H.; Welch, J.; Zastrau, U.; Neumayer, P.; Hastings, J. B.; Glenzer, S. H. Ultrabright X-ray laser scattering for dynamic warm dense matter physics. *Nat. Photonics* **2015**, *9*, 274.

(8) Mermin, N. D. Thermal Properties of the Inhomogeneous Electron Gas. *Phys. Rev.* **1965**, *137*, A1441–A1443.

(9) Zhang, S.; Driver, K. P.; Soubiran, F.; Militzer, B. First-principles equation of state and shock compression predictions of warm dense hydrocarbons. *Phys. Rev. E* **2017**, *96*, 013204.

(10) Karasiev, V. V.; Calderín, L.; Trickey, S. B. Importance of finite-temperature exchange correlation for warm dense matter calculations. *Phys. Rev. E* **2016**, *93*, 063207.

(11) Karasiev, V. V.; Sjostrom, T.; Dufty, J.; Trickey, S. B. Accurate Homogeneous Electron Gas Exchange-Correlation Free Energy for Local Spin-Density Calculations. *Phys. Rev. Lett.* **2014**, *112*, 076403.

(12) Groth, S.; Dornheim, T.; Sjostrom, T.; Malone, F. D.; Foulkes, W. M. C.; Bonitz, M. Ab initio Exchange-Correlation Free Energy of the Uniform Electron Gas at Warm Dense Matter Conditions. *Phys. Rev. Lett.* **2017**, *119*, 135001.

(13) Karasiev, V. V.; Hu, S. X.; Zaghou, M.; Boehly, T. R. Exchange-correlation thermal effects in shocked deuterium: Softening the principal Hugoniot and thermophysical properties. *Phys. Rev. B* **2019**, *99*, 214110.

(14) Mermin, N. D. Stability of the thermal Hartree-Fock approximation. *Ann. Phys.* **1963**, *21*, 99–121.

(15) Kou, Z.; Hirata, S. Finite-temperature full configuration interaction. *Theoretical Chemistry Accounts* **2014**, *133*.

(16) He, X.; Ryu, S.; Hirata, S. Finite-temperature second-order many-body perturbation and HartreeFock theories for one-dimensional solids: An application to Peierls and charge-density-wave transitions in conjugated polymers. *The Journal of Chemical Physics* **2014**, *140*, 024702.

(17) Hermes, M. R.; Hirata, S. Finite-temperature coupled-cluster, many-body perturbation, and restricted and unrestricted HartreeFock study on one-dimensional solids: Luttinger liquids, Peierls transitions, and spin- and charge-density waves. *The Journal of Chemical Physics* **2015**, *143*, 102818.

(18) Rusakov, A. A.; Zgid, D. Self-consistent second-order Greens function perturbation theory for periodic systems. *The Journal of Chemical Physics* **2016**, *144*, 054106.

(19) Hummel, F. Finite Temperature Coupled Cluster Theories for Extended Systems. *Journal of Chemical Theory and Computation* **2018**, *14*, 6505–6514.

(20) White, A. F.; Chan, G. K.-L. A Time-Dependent Formulation of Coupled-Cluster The-

ory for Many-Fermion Systems at Finite Temperature. *Journal of Chemical Theory and Computation* **2018**, *14*, 5690–5700.

(21) Harsha, G.; Henderson, T. M.; Scuseria, G. E. Thermofield theory for finite-temperature quantum chemistry. *The Journal of Chemical Physics* **2019**, *150*, 154109.

(22) Harsha, G.; Henderson, T. M.; Scuseria, G. E. Thermofield theory for finite-temperature coupled cluster. *Journal of Chemical Theory and Computation* **2019**,

(23) Sanyal, G.; Mandal, S. H.; Mukherjee, D. Thermal averaging in quantum many-body systems: a non-perturbative thermal cluster cumulant approach. *Chemical Physics Letters* **1992**, *192*, 55–61.

(24) Ceperley, D. M. Path integrals in the theory of condensed helium. *Rev. Mod. Phys.* **1995**, *67*, 279–355.

(25) Driver, K. P.; Militzer, B. All-Electron Path Integral Monte Carlo Simulations of Warm Dense Matter: Application to Water and Carbon Plasmas. *Phys. Rev. Lett.* **2012**, *108*, 115502.

(26) Driver, K. P.; Soubiran, F.; Zhang, S.; Militzer, B. First-principles equation of state and electronic properties of warm dense oxygen. *The Journal of Chemical Physics* **2015**, *143*, 164507.

(27) Ceperley, D. M. Fermion nodes. *J. Stat. Phys.* **1991**, *63*, 1237–1267.

(28) Foulkes, W. M. C.; Mitas, L.; Needs, R. J.; Rajagopal, G. Quantum Monte Carlo simulations of solids. *Reviews of Modern Physics* **2001**, *73*, 33–83.

(29) Brown, E. W.; Clark, B. K.; DuBois, J. L.; Ceperley, D. M. Path-Integral MonteCarlo Simulation of the Warm Dense Homogeneous Electron Gas. *Phys. Rev. Lett.* **2013**, *110*, 146405.

(30) Schoof, T.; Groth, S.; Vorberger, J.; Bonitz, M. \textit{Ab Initio} Thermodynamic Results for the Degenerate Electron Gas at Finite Temperature. *Phys. Rev. Lett.* **2015**, *115*, 130402.

(31) Malone, F. D.; Blunt, N.; Brown, E. W.; Lee, D.; Spencer, J.; Foulkes, W.; Shepherd, J. J. Accurate Exchange-Correlation Energies for the Warm Dense Electron Gas. *Physical Review Letters* **2016**, *117*.

(32) Dornheim, T.; Groth, S.; Filinov, A.; Bonitz, M. Permutation blocking path integral Monte Carlo: a highly efficient approach to the simulation of strongly degenerate non-ideal fermions. *New J. of Phys.* **2015**, *17*, 73017.

(33) DuBois, J. L.; Brown, E. W.; Alder, B. J. *Advances in the Computational Sciences*; Chapter Chapter 13, pp 184–192.

(34) Schoof, T.; Bonitz, M.; Filinov, A.; Hochstuhl, D.; Dufty, J. W. Configuration Path Integral Monte Carlo. *Contr. Plasma Phys.* **2011**, *51*, 687–697.

(35) Blankenbecler, R.; Scalapino, D. J.; Sugar, R. L. Monte Carlo calculations of coupled boson-fermion systems. I. *Phys. Rev. D* **1981**, *24*, 2278–2286.

(36) Scalapino, D. J.; Sugar, R. L. Method for Performing Monte Carlo Calculations for Systems with Fermions. *Phys. Rev. Lett.* **1981**, *46*, 519–521.

(37) Zhang, S. Finite-Temperature Monte Carlo Calculations for Systems with Fermions. *Phys. Rev. Lett.* **1999**, *83*, 2777–2780.

(38) Rubenstein, B. M.; Zhang, S.; Reichman, D. R. Finite-temperature auxiliary-field quantum Monte Carlo technique for Bose-Fermi mixtures. *Phys. Rev. A* **2012**, *86*, 053606.

(39) LeBlanc, J. P. F.; Antipov, A. E.; Becca, F.; Bulik, I. W.; Chan, G. K.-L.; Chung, C.-M.; Deng, Y.; Ferrero, M.; Henderson, T. M.; Jiménez-Hoyos, C. A.; Kozik, E.; Liu, X.-W.; Millis, A. J.; Prokof'ev, N. V.; Qin, M.; Scuseria, G. E.; Shi, H.; Svistunov, B. V.;

Tocchio, L. F.; Tupitsyn, I. S.; White, S. R.; Zhang, S.; Zheng, B.-X.; Zhu, Z.; Gull, E. Solutions of the Two-Dimensional Hubbard Model: Benchmarks and Results from a Wide Range of Numerical Algorithms. *Phys. Rev. X* **2015**, *5*, 041041.

(40) Motta, M.; Ceperley, D. M.; Chan, G. K.-L.; Gomez, J. A.; Gull, E.; Guo, S.; Jimnez-Hoyos, C. A.; Lan, T. N.; Li, J.; Ma, F.; Millis, A. J.; Prokofev, N. V.; Ray, U.; Scuseria, G. E.; Sorella, S.; Stoudenmire, E. M.; Sun, Q.; Tupitsyn, I. S.; White, S. R.; Zgid, D.; Zhang, S.; Simons Collaboration on the Many-Electron Problem, Towards the Solution of the Many-Electron Problem in Real Materials: Equation of State of the Hydrogen Chain with State-of-the-Art Many-Body Methods. *Physical Review X* **2017**, *7*.

(41) Motta, M.; Zhang, S. Ab initio computations of molecular systems by the auxiliary-field quantum Monte Carlo method. *WIREs Comput. Mol. Sci.* **2018**, *8*, e1364.

(42) Zhang, S.; Krakauer, H. Quantum Monte Carlo Method using Phase-Free Random Walks with Slater Determinants. *Phys. Rev. Lett.* **2003**, *90*, 136401.

(43) Liu, Y.; Cho, M.; Rubenstein, B. *Ab Initio* Finite Temperature Auxiliary Field Quantum Monte Carlo. *Journal of Chemical Theory and Computation* **2018**, *14*, 4722–4732.

(44) Blunt, N. S.; Rogers, T. W.; Spencer, J. S.; Foulkes, W. M. C. Density-matrix quantum Monte Carlo method. *Physical Review B* **2014**, *89*.

(45) Booth, G. H.; Thom, A. J. W.; Alavi, A. Fermion Monte Carlo without fixed nodes: A game of life, death, and annihilation in Slater determinant space. *The Journal of Chemical Physics* **2009**, *131*, 054106.

(46) Malone, F. D.; Blunt, N. S.; Shepherd, J. J.; Lee, D. K. K.; Spencer, J. S.; Foulkes, W. M. C. Interaction picture density matrix quantum Monte Carlo. *The Journal of Chemical Physics* **2015**, *143*, 044116.

(47) Cleland, D.; Booth, G. H.; Alavi, A. Communications: Survival of the fittest: Accelerating convergence in full configuration-interaction quantum Monte Carlo. *The Journal of Chemical Physics* **2010**, *132*, 041103.

(48) Petruzielo, F. R.; Holmes, A. A.; Changlani, H. J.; Nightingale, M. P.; Umrigar, C. J. Semistochastic Projector Monte Carlo Method. *Physical Review Letters* **2012**, *109*.

(49) Blunt, N. S.; Smart, S. D.; Kersten, J. A. F.; Spencer, J. S.; Booth, G. H.; Alavi, A. Semi-stochastic full configuration interaction quantum Monte Carlo: Developments and application. *The Journal of Chemical Physics* **2015**, *142*, 184107.

(50) Holmes, A. A.; Changlani, H. J.; Umrigar, C. J. Efficient Heat-Bath Sampling in Fock Space. *Journal of Chemical Theory and Computation* **2016**, *12*, 1561–1571.

(51) Li, J.; Otten, M.; Holmes, A. A.; Sharma, S.; Umrigar, C. J. Fast semistochastic heat-bath configuration interaction. *The Journal of Chemical Physics* **2018**, *149*, 214110.

(52) Blunt, N. S. Communication: An efficient and accurate perturbative correction to initiator full configuration interaction quantum Monte Carlo. *The Journal of Chemical Physics* **2018**, *148*, 221101.

(53) Blunt, N. S.; Thom, A. J. W.; Scott, C. J. C. Preconditioning and Perturbative Estimators in Full Configuration Interaction Quantum Monte Carlo. *Journal of Chemical Theory and Computation* **2019**, *15*, 3537–3551.

(54) Deustua, J. E.; Magoulas, I.; Shen, J.; Piecuch, P. Communication: Approaching exact quantum chemistry by cluster analysis of full configuration interaction quantum Monte Carlo wave functions. *The Journal of Chemical Physics* **2018**, *149*, 151101.

(55) Deustua, J. E.; Yuwono, S. H.; Shen, J.; Piecuch, P. Accurate excited-state energetics by a combination of Monte Carlo sampling and equation-of-motion coupled-cluster computations. *The Journal of Chemical Physics* **2019**, *150*, 111101.

(56) Shen, J.; Piecuch, P. Combining active-space coupled-cluster methods with moment energy corrections via the CC(P ; Q) methodology, with benchmark calculations for biradical transition states. *The Journal of Chemical Physics* **2012**, *136*, 144104.

(57) Bauman, N. P.; Shen, J.; Piecuch, P. Combining active-space coupled-cluster approaches with moment energy corrections via the CC(P ; Q) methodology: connected quadruple excitations. *Molecular Physics* **2017**, *115*, 2860–2891.

(58) Deustua, J. E.; Shen, J.; Piecuch, P. Converging High-Level Coupled-Cluster Energetics by Monte Carlo Sampling and Moment Expansions. *Physical Review Letters* **2017**, *119*.

(59) Booth, G. H.; Grüneis, A.; Kresse, G.; Alavi, A. Towards an exact description of electronic wavefunctions in real solids. *Nature* **2013**, *493*, 365–370.

(60) Cleland, D. The initiator Full Configuration Interaction Quantum Monte Carlo method: Development and applications to molecular systems. Ph.D. thesis, University of Cambridge, 2009.

(61) Spencer, J. S.; Blunt, N. S.; Choi, S.; Etrych, J.; Filip, M.-A.; Foulkes, W. M. C.; Franklin, R. S. T.; Handley, W. J.; Malone, F. D.; Neufeld, V. A.; Di Remigio, R.; Rogers, T. W.; Scott, C. J. C.; Shepherd, J. J.; Vigor, W. A.; Weston, J.; Xu, R.; Thom, A. J. W. The HANDE-QMC Project: Open-Source Stochastic Quantum Chemistry from the Ground State Up. *Journal of Chemical Theory and Computation* **2019**, *15*, 1728–1742.

(62) Sun, Q.; Berkelbach, T. C.; Blunt, N. S.; Booth, G. H.; Guo, S.; Li, Z.; Liu, J.; McClain, J. D.; Sayfutyarova, E. R.; Sharma, S.; Wouters, S.; Chan, G. K.-L. PySCF: the Python-based simulations of chemistry framework. *Wiley Interdiscip. Rev.: Comput. Mol. Sci.* **2018**, *8*, e1340.

(63) Werner, H.-J.; Knowles, P. J.; Knizia, G.; Manby, F. R.; Schütz, M. Molpro: a general-

purpose quantum chemistry program package. *WIREs Comput Mol Sci* **2012**, *2*, 242–253.

(64) Poole, T. Calculating derivatives within quantum Monte Carlo. Ph.D. thesis, Imperial College London, 2015.

(65) Cleland, D.; Booth, G. H.; Overy, C.; Alavi, A. Taming the First-Row Diatomics: A Full Configuration Interaction Quantum Monte Carlo Study. *Journal of Chemical Theory and Computation* **2012**, *8*, 4138–4152.